Post-print version: Jimenez-Vicaria, J. D., G. Pulido, M. D., & Castro-Fresno, D. (2020). Influence of carbon fibre stiffness and adhesive ductility on CFRP-steel adhesive joints with short bond lengths. Construction and Building Materials, 260 doi:10.1016/j.conbuildmat.2020.119758

Influence of carbon fibre stiffness and adhesive ductility on CFRP-steel adhesive joints with short bond lengths

Jimenez-Vicaria, J. David[1, 2*]; G. Pulido, M. Dolores[3]; Castro-Fresno, Daniel[4]

1: Centro Tecnológico. ACCIONA Construcción. Valportillo Segunda 8, 28108 Alcobendas (Spain)
e-mail (corresponding author*): josedavid.jimenez.vicaria@acciona.com

2: GITECO. Universidad de Cantabria. Avda. de los Castros 44, 39005 Santander (Spain)
e-mail: jose-david.jimenez@alumnos.unican.es

3: Instituto CC Eduardo Torroja – CSIC. Serrano Galvache 4, 28033 Madrid (Spain)
e-mail: dpulido@ietcc.csic.es

4: GITECO. Universidad de Cantabria. Avda. de los Castros 44, 39005 Santander (Spain)
e-mail: castrod@unican.es

Abstract

The use of adhesively-bonded CFRP laminates is a promising technique to strengthen steel structures that have been deteriorated due to corrosion, ageing or increasing loads, as in the case of old metallic riveted bridges. But the relatively short available space between rivets requires the use of adhesively-bonded CFRP laminates with short bond lengths, which needs to be deeply studied as most previous research works have focused on large bond lengths. To study the bond behaviour between CFRP laminates and steel plates in such strengthened structures, a series of tests has been carried out in double-strap joints under tensile loading, evaluating the influence of CFRP stiffness and adhesive ductility on the strength and failure mode of short bond length adhesive joints. Based on the experimental results of the present work, together with a large database collected from literature, a fracture-mechanics model based on interfacial fracture energy in shear G_{II} is calibrated, and a simple expression is developed to be used in design for the strength prediction of such adhesive joints. Finally, double-strap joint specimens are simulated using cohesive zone models (CZM) for the adhesive layers, and the results are compared to the analytical model and experimental tests.

***Keywords*:** Carbon fibre reinforced polymer; CFRP-steel adhesive joints; Mechanical testing; Fracture mechanics; Finite element analysis; cohesive zone models.

1. Introduction

Old metallic railway bridges are subject to a large number of cyclic high loads during their service life, so many of them experience fatigue damage in certain construction details as a consequence of high stress concentrations. To extend the service life of these structures, the stress levels in those fatigue-prone details need to be reduced by the application of strengthening strategies. In recent years, there has been a large interest in the use of carbon fibre reinforced polymers (CFRP) laminates for steel bridge strengthening. These laminates can be installed adhesively bonded to the steel surface, or as prestressed unbonded plates with the ends fixed to the metallic girders using friction clamps, rather than adhesive bonding [1, 2]. The present work focuses on the adhesively-bonded method, as it is an excellent alternative to traditional techniques, such as welded or bolted steel plates [3]. It is particularly interesting in the case of riveted old metallic bridges, since welding the original metal is not always possible, and drilling holes for bolting can increase localised stresses weakening the structure [4]. Additionally, steel plates add extra weight and can suffer from corrosion increasing future maintenance costs, while CFRP laminates have a high strength-to-weight ratio and are resistant to harsh environments. Although creep in adhesive bonds could be an issue if the joint is going to be under large sustained loads [5, 6], this is not the case for fatigue strengthening, as loads on the joint are mainly variable (cyclic live loads).

One drawback of adhesively-bonded CFRP laminates for the strengthening of riveted metallic structures is the relatively short available length between rivets to bond the CFRP laminates (usually few centimetres). For this reason, the study of CFRP-metal adhesively-bonded joints when the bond length is short is found interesting, since most previous research works have focused on the behaviour of large bond lengths [7, 8, 9]. In fact, most experimental works assume that the effective bond length L_e (the bond length beyond which the joint strength does not increase) is guaranteed by using large bond lengths in the joint, and also in some cases the yielding strain in the steel plate is attained before the joint failure [10, 11], what is not desirable under the service loads related to fatigue.

For a suitable use of this innovative technology, the behaviour of the bond between the CFRP laminate and the metallic element to be strengthened needs to be deeply studied. This can be done by testing CFRP-metal double-strap joints [12, 13, 14, 15, 16, 17], which are formed by two CFRP laminates bonded with adhesive to both sides of two metallic plates aligned and separated by a gap, simulating a metallic element with a fatigue crack. As previously reported in [18], there are six failure modes that can occur in this type of adhesive joints: a) adhesive failure in the steel-adhesive interface; b) adhesive failure in the CFRP-adhesive interface; c) cohesive failure (rupture of the adhesive); d) delamination in the CFRP (separation of some carbon fibres from the resin matrix); e) rupture of the CFRP and f) steel yielding. For the adoption of a proper model to predict the joint strength, the failure mode must be considered.

Several analytical models are proposed in literature to predict the strength of these double-strap joints [19, 20, 21], but basically they can be grouped into two different failure criteria: continuum mechanics (stress or strain-based models) and fracture mechanics (fracture energy-based models). Regarding stress or strain-based models, Hart-Smith analytical model [22] has been commonly used in literature to predict the failure load P_u in double-strap joint specimens [23, 24, 25]. This model was developed for the analysis of

joints with elastic-perfect plastic behaviour of the adhesive in shear that fail with a cohesive failure mode (rupture of the adhesive), so the plastic shear strain γ_p of the adhesive is a fundamental parameter in this model. In this sense, some experimental works [23, 24, 25, 26] have focused on the determination of γ_p based on experimental results of double-strap joint tests. However, in most cases, especially for short bond lengths [7, 12, 27, 28], the failure mode is adhesive (at the steel-adhesive or CFRP-adhesive interface), showing an elastic behaviour of the joint until failure, so authors find that is not convenient to use Hart-Smith analytical model for the prediction of bond strength in these cases. Consequently, fracture mechanics approach is found more suitable to predict the debonding strength of double-strap joint specimens with short bond lengths.

The mechanical properties of the materials used for the strengthening system (CFRP and adhesive) play an important role in the behaviour of these joints, as previously reported by [29] and [30], and the present work focuses specially on the CFRP stiffness and the adhesive ductility. To evaluate the influence of these parameters on the behaviour of double-strap joints with short bond lengths, two different carbon fibres (FC230 and FC390) and two epoxy adhesives (EP1 and EP2) are studied in the present work, so that the most efficient combination of strengthening materials can be found for this particular case. Also, two different short bond lengths L_1 have been used for the double-strap joint at one side of the gap (L_1 = *30 mm and* L_1 = *60 mm*), being the bond length L_2 of the joint at the other side of the gap 50 % larger than L_1, to try to make sure that the failure during testing takes place on the shortest side of the joint.

From the experimental results, a fracture-mechanics based analytical model is calibrated and a simple expression is developed to be used in design for the strength prediction of double-strap CFRP-steel joints. Likewise, numerical models with finite elements are performed and results are compared to those obtained from the analytical model.

2. Experimental program

2.1 Specimen preparation and test set-up

A total of 28 double-strap joint tests were carried out, 7 specimens for each combination of adhesive and carbon fibre: EP1-FC230, EP1-FC390, EP2-FC230 and EP2-FC390. For each group of 7 specimens, three had a bond length of L_1 = *30 mm* and the other four had a length of L_1 = *60 mm* (Fig. 1). All test specimens were fabricated with an adhesive nominal thickness t_a of 0.5 mm, except a specimen with L_1 = *60 mm* for each combination of adhesive and carbon fibre (4 test specimens), which was manufactured with a greater thickness (t_a = *2.0 mm*) to evaluate its effect on the strength of the joint. For each combination of bond length, adhesive and carbon fibre, three identical specimen repetitions were tested.

The nomenclature used for each specimen begins with the bond length L_1 (L30 or L60), followed by the adhesive type (EP1 or EP2), the carbon fibre used (FC230 or FC390) and finally a number to differentiate between repetitions (S1, S2 or S3). For example, the specimen L60-EP2-FC390-S2 refers to the second specimen with bond length L_1 = *60 mm*, epoxy adhesive EP2, and carbon fibre FC390.

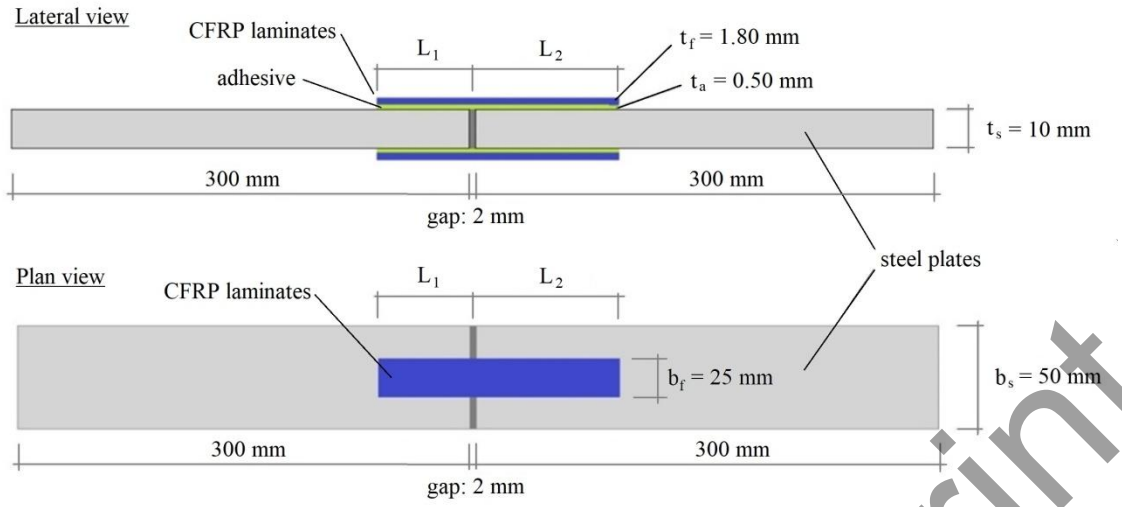

Fig. 1. Schematic view of the CFRP-steel double-strap joint specimens (dimensions are not to scale).

To prepare the double-strap joint specimens, first the surface of steel plates was grit blasted with aluminium silica, since it has been demonstrated to be the most effective surface treatment for the steel [31, 32]. After that, two steel plates were aligned, maintaining a gap of 2 mm between them by means of a neoprene joint, and subsequently an adhesive layer was applied uniformly on both the surface of the steel and the CFRP laminate. Next, the CFRP laminate was positioned on the surface of the steel plate, and pressure was applied to remove the excess of adhesive, until the desired adhesive thickness was achieved. To control the correct alignment of the specimen and the thickness of the adhesive, an alignment tool and a series of separators were used to maintain a fixed thickness of adhesive during the preparation (Fig. 2a). One specimen per combination of parameters was instrumented by strain gauges attached to the CFRP to measure the strains in the CFRP laminates during loading (Fig. 2b), which are then compared with those obtained in the numerical models. All tests were carried out in tensile using an Instron 3382 multitest press, in displacement control at a loading rate of 0.5 mm/min until failure. Fig. 3 shows one specimen tested for each bond length L_1.

a) Bonding of CFRP laminates b) Instrumentation with strain gauges

Fig. 2. Preparation of CFRP-steel double-strap joints.

a) L_1 = *30 mm* b) L_1 = *60 mm*

Fig. 3. Tensile tests in CFRP-steel double-strap joints.

2.2 Material properties

The steel plates used were manufactured from hot rolled structural steel S275 JR, with yield stress, tensile strength and failure strain of 310 MPa, 450 MPa and 37.2%, respectively, according to the manufacturer. The plates had a length, width and thickness of 300 mm, 50 mm and 10 mm, respectively (Fig. 1). The dimensions of the steel plates were selected so that the steel does not yield during the test.

CFRP laminates of 1.80 mm nominal thickness and 25 mm width were used (Figure 1), manufactured by resin infusion with a two-part epoxy resin (Araldite LY 1568/Aradur 3489) on unidirectional carbon fibre fabrics with *Toray T700* fibres (FC230 laminates) and *Pyrofil HR40* fibres (FC390 laminates). From tensile tests on standardized specimens according to ASTM-D3039 [33], the modulus of elasticity E_f, tensile strength $f_{t,f}$, strain at failure $\varepsilon_{t,f}$ and Poisson coefficient v_f of CFRP laminates were experimentally determined, obtaining average values of 117146 MPa, 1932 MPa, 1.65 % and 0.322 for FC230 laminates (4 specimens tested), and average values of 183605 MPa, 1663 MPa, 0.91 % and 0.328 for FC390 laminates (3 specimens tested), respectively (Table 1).

As structural epoxy adhesives for bonding the CFRP laminates to the steel plates, Araldite AW 4856 (EP1) and Araldite 2031 (EP2) were used, and their mechanical properties were obtained experimentally from tensile tests (ASTM-D638 standard [34]) with an average modulus of elasticity E_a, tensile strength $f_{t,a}$ and ultimate tensile strain $\varepsilon_{t,a}$ of 4951 MPa, 30 MPa and 0.62 % for EP1 (5 specimens tested), and 1451 MPa, 19 MPa and 2.98 % for EP2 (4 specimens tested), respectively. The tensile strain energy R_a of each adhesive (area under the uniaxial tensile stress-strain curve) is 0.09 MPa mm/mm for EP1 and 0.37 MPa mm/mm for EP2 (Fig. 4b).

As it can be observed in the tensile stress-strain curves of Fig. 4, the two CFRP laminates have different tensile axial stiffness, being FC390 57 % stiffer than FC230. In the case of epoxy adhesives, EP1 is 3.4 times stiffer than EP2 (in the elastic range), but the most relevant difference is that EP1 is elastic until failure (fragile behaviour), while EP2 has a ductile behaviour with larger deformation up to failure, with a tensile strain energy 4 times higher than EP1.

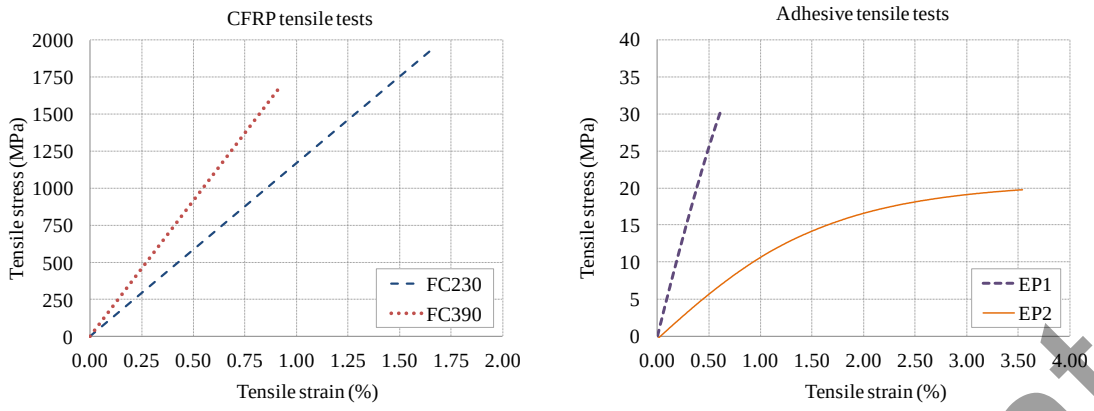

a) CFRP b) Adhesive

Fig. 4. Tensile tests on strengthening materials.

The average measured material properties of CFRP and adhesives are listed in Table 1 along with those of steel plates reported by the manufacturer. The mechanical properties of each material specimen tested (CFRP and adhesive) is presented in Table 2 and Table 3.

Table 1. Material properties of CFRP, adhesives and steel (average values).

	FC230	FC390	EP1	EP2	Steel**
Tensile strength (MPa)	1932	1663	30	19	450
Yield strength (MPa)	-	-	-	-	310
Tensile modulus (MPa)	117146	183605	4951	1451	200000
Failure strain (%)	1.65	0.91	0.61	2.98	37.20
Poisson ratio	0.322	0.328	0.350*	0.350*	0.300

Assumed values (not measured during tests)

***Properties supplied by manufacturer*

Table 2. Material properties of CFRP specimens tested.

Specimen	$f_{t,f}$ (MPa)	E_f (MPa)	$\varepsilon_{t,f}$ (%)	υ_f
FC230 - 1	2060	123036	1.67	0.328
FC230 - 2	1789	107509	1.66	0.290
FC230 - 3	1971	120271	1.64	0.284
FC230 - 4	1908	117769	1.62	0.385
Mean	1932	117146	1.65	0.322
COV (%)	5.9	5.8	1.5	14.4
FC390 -1	1571	175988	0.89	0.331
FC390 -2	1626	195119	0.83	0.340
FC390 -3	1791	179708	1.00	0.314
Mean	1663	183605	0.91	0.328
COV (%)	6.9	5.5	9.1	4.0

Table 3. Material properties of adhesive specimens tested.

Specimen	$f_{t,a}$ (MPa)	E_a (MPa)	$\varepsilon_{t,a}$ (%)
EP1 - 1	36	4801	0.75
EP1 - 2	37	4614	0.80
EP1 - 3	29	5025	0.58
EP1 - 4	26	5415	0.48
EP1 - 5	22	4900	0.45
Mean	30	4951	0.61
COV (%)	21.3	6.1	25.7
EP2 - 1	17	1407	2.00
EP2 - 2	21	1420	3.20
EP2 - 3	20	1692	3.30
EP2 - 4	18	1287	3.40
Mean	19	1451	2.98
COV (%)	9.0	11.8	22.0

3. Experimental results

The experimental results are summarized in Table 4 and Table 5, in which for each test, the failure load $P_{u,\,test}$, the elongation of the specimen measured at failure δ_u and the stiffness of the joint K, obtained from the slope of the *load P [kN] - elongation δ [mm]* curve in the elastic range during the test (Fig. 5a for EP1 and Fig. 5b for EP2), are presented. Table 4 and Table 5 also show the failure mode of the specimen, the theoretical interfacial fracture energy in shear G_{II}, the theoretical strength of the joint $P_{u,\,theo}$ (calculated from the fracture mechanics strength model presented below) and the failure load from the numerical models.

Table 4. Experimental results of the CFRP-steel double-strap joint tests with bond length $L_1 = 30$ *mm*.

L_1 (mm)	Adh.	Carbon fibre	Spec.	$P_{u,test}$ (kN)	δ_u (mm)	K (kN/mm)	G_{II} (N/mm)	$P_{u,theo}$ (kN)	$P_{u,test}/P_{u,theo}$	$P_{u,FEM}$ (kN)	$P_{u,FEM}/P_{u,theo}$	Failure mode [c]
30	EP1	FC230	S1[b]	42.18	2.07	20.24	0.56	25.83	1.63	19.24	0.74	A
			S2	42.10	2.16	19.28	0.56	26.15	1.61	-	-	A
			S3	35.81	1.90	18.85	0.60	24.98	1.43	-	-	A
			Average	40.03	2.04	19.46	0.57	25.65	1.56	-	-	-
			COV	0.09	0.06	0.04	0.04	0.02	0.07	-	-	-
30	EP1	FC390	S1	34.81	1.80	19.48	0.53	31.48	1.11	-	-	A
			S2	35.07	1.82	19.33	0.53	31.39	1.12	-	-	A
			S3[b]	36.34	1.85	19.84	0.53	31.46	1.16	23.44	0.75	A
			Average	35.41	1.82	19.55	0.53	31.44	1.13	-	-	-
			COV	0.02	0.01	0.01	0.00	0.00	0.02	-	-	-
30	EP2	FC230	S1	28.80	1.67	17.78	0.72	26.79	1.08	-	-	A
			S2[b]	24.85	1.62	16.34	0.75	26.21	0.95	19.52	0.74	A
			S3	26.85	1.58	17.33	0.73	26.62	1.01	-	-	A
			Average	26.83	1.62	17.15	0.73	26.54	1.01	-	-	-

			COV	0.07	0.03	0.04	0.02	0.01	0.06	-	-	-
			S1[b]	29.67	1.57	19.42	0.68	33.04	0.90	21.91	0.66	A
			S2	27.86	1.62	17.62	0.66	33.37	0.83	-	-	A
30	EP2	FC390	S3	27.88	1.50	18.71	0.69	32.27	0.86	-	-	A
			Average	28.47	1.56	18.58	0.68	32.89	0.86	-	-	-
			COV	0.04	0.04	0.05	0.02	0.02	0.04	-	-	-

b. Specimens instrumented with strain gauges; c. Failure mode: A (adhesive) and C (mixed cohesive-adhesive).

Table 5. Experimental results of the CFRP-steel double-strap joint tests with bond length $L_1 = 60$ *mm*.

L_1 *(mm)*	*Adh.*	*Carbon fibre*	*Spec.*	$P_{u,test}$ *(kN)*	δ_u *(mm)*	K *(kN/mm)*	G_{II} *(N/mm)*	$P_{u,theo}$ *(kN)*	$P_{u,test}/P_{u,theo}$	$P_{u,FEM}$ *(kN)*	$P_{u,FEM}/P_{u,theo}$	*Failure mode* [c]
			S1[b]	32.67	1.72	19.36	1.22	36.46	0.90	38.84	1.07	C
			S2	43.51	2.32	18.53	1.19	37.03	1.18	-	-	C
60	EP1	FC230	S3	46.02	2.32	19.64	1.19	37.69	1.22	-	-	C
			Average	40.73	2.12	19.18	1.20	37.06	1.10	-	-	-
			COV	0.17	0.16	0.03	0.01	0.02	0.16	-	-	-
			S1[b]	60.24	2.91	19.83	1.07	46.50	1.30	46.78	1.01	C
			S2	58.18	2.80	19.98	1.06	47.39	1.23	-	-	C
60	EP1	FC390	S3	52.35	2.52	20.09	1.08	47.33	1.11	-	-	C
			Average	56.92	2.74	19.97	1.07	47.07	1.21	-	-	-
			COV	0.07	0.07	0.01	0.01	0.01	0.08	-	-	-
			S1	57.66	3.07	19.95	1.61	42.08	1.37	-	-	C
			S2[b]	56.33	2.99	19.84	1.58	41.32	1.36	39.24	0.95	C
60	EP2	FC230	S3	59.23	3.31	18.66	1.56	42.30	1.40	-	-	C
			Average	57.74	3.12	19.48	1.58	41.90	1.38	-	-	-
			COV	0.03	0.05	0.04	0.02	0.01	0.02	-	-	-
			S1	63.63	3.20	21.17	1.44	51.23	1.24	-	-	C
			S2	63.25	3.18	20.86	1.46	51.79	1.22	-	-	C
60	EP2	FC390	S3[b]	58.66	2.97	21.00	1.40	51.24	1.14	50.15	0.98	C
			Average	61.85	3.12	21.01	1.43	51.42	1.20	-	-	-
			COV	0.04	0.04	0.01	0.02	0.01	0.04	-	-	-
60	EP1[a]	FC230	S1_2[b]	43.14	2.15	19.90	1.36	40.71	1.06	38.84	0.95	C
		FC390	S1_2[b]	51.10	2.46	20.30	1.26	50.90	1.00	46.78	0.92	C
60	EP2[a]	FC230	S1_2[b]	49.57	2.82	19.05	1.85	42.27	1.17	39.24	0.93	C
		FC390	S1_2[b]	48.41	2.63	19.86	1.73	48.86	0.99	50.15	1.03	C

Notes: a. Adhesive thickness $t_a = 2.0$ mm; b. Specimens instrumented with strain gauges; c. Failure mode: A (adhesive) and C (mixed cohesive-adhesive).

In the case of the joint strength, for the specimen geometry tested (bond lengths and adhesive thicknesses used), the highest strength ($P_{max} = 63.63$ *kN*) was obtained for bond length $L_1 = 60$ *mm* using adhesive EP2 and carbon fibre FC390, with adhesive thickness of 0.50 mm. However, in this case, the failure load was only 7 % higher compared to the same specimen with FC230. A similar increase (6 %) was reported when changing from FC230 to FC390 for bond length $L_1 = 30$ *mm* with EP2 adhesive. Therefore, it can be concluded that in the case of using EP2 adhesive (ductile adhesive), the joint strength was hardly

increased by using a stiffer carbon fibre (FC 390). One reason for this can be that, in the case of the short bond lengths tested, the maximum strength of the joint was not attained (the effective bond length L_e is expected to be higher than $L_1 = 60\ mm$), so the ductile behaviour of the adhesive EP2 was not fully developed.

However, when using EP1 adhesive, the strength increased 40 % when going from FC230 to FC 390 for bond length $L_1 = 60\ mm$, while it decreased by 13 % for bond length $L_1 = 30\ mm$. In this case, it can be concluded that when using adhesive EP1 (fragile adhesive), it is convenient to use a stiffer carbon fibre in the case of bond length $L_1 = 60\ mm$, not being so for bond lengths shorter, such as $L_1 = 30\ mm$. Based on a previous experimental work by the authors with similar EP1 specimens and bond lengths $L_1 = 50\ mm$ and $L_1 = 100\ mm$ [31], it could be expected that L_e was around 50-60 mm for these specimens with EP1, so the maximum strength of the joint was attained for $L_1 = 60\ mm$.

For short bond lengths $L_1 = 30\ mm$, the increase of adhesive ductility (changing from EP1 to EP2) reduced the joint strength 49% and 24% when using FC230 and FC390, respectively (the strength reduction was more pronounced when using FC230). On the contrary, for bond lengths $L_1 = 60\ mm$, the increase of adhesive ductility (changing from EP1 to EP2) increased the joint strength 42% and 9% when using FC230 and FC390, respectively (the strength increase was more pronounced when using FC230).

In case of short bond lengths $L_1 = 30\ mm$ must be used (for example, due to lack of space in the element to be strengthened), the highest strengths were obtained with adhesive EP1 (fragile) and carbon fibre FC230 (less stiff fibre), with 49 % higher failure load than that obtained with the same carbon fibre (FC230) and ductile adhesive (EP2).

Therefore, the use of one type or another of carbon fibre and adhesive will be motivated by the geometrical restrictions of the detail to be strengthened, especially by the available length to bond the CFRP patches to strengthen the metallic element. For short bond lengths ($L_1 = 30\ mm$) it is better to use EP1 adhesive with FC230 carbon fibre, while for longer bond lengths ($L_1 = 60\ mm$) EP2 adhesive with FC390 carbon fibre could be more efficient.

As shown in Table 4 and Table 5, the stiffness of the joint was similar in all tests (between 17.15 and 21.01 kN/mm), regardless of the bond length L_1, the CFRP or the adhesive used, although it was slightly higher when using a stiffer carbon fibre (FC 390) and longer bond lengths ($L_1 = 60\ mm$) in the case of ductile adhesive EP2. With ductile adhesive (EP2) and $L_1 = 30\ mm$, the effect of CFRP stiffness is clear on the slope of the load-elongation curve. In this case, the failure load was slightly higher for FC390, but the elongation at failure was smaller than in specimen with FC230.

In some experimental works carried out by other authors [7, 8, 9], bond lengths were long enough to develop the maximum strength of the joint (that is to say, the bond length was higher than the effective bond length L_e). Also, sometimes the steel yielded before the failure of the adhesive joint [10, 35], so in some cases the load-elongation curves showed a ductile behaviour (after reaching the maximum load, the force could not increase anymore but the specimen was still able to withstand displacement increments showing a plateau). For EP2 specimens the bond length $L_1 = 60\ mm$ was assumed to be shorter than L_e, and also the steel remained elastic until joint failure (as measured by strain gauges), so the ductile behaviour observed in other research works [10, 35] was not observed in this case. If $L_1 < L_e$, the

maximum force P_{max} cannot be transferred and the rupture is of brittle type, i.e., without any horizontal plateau, as it can be seen in Fig. 5.

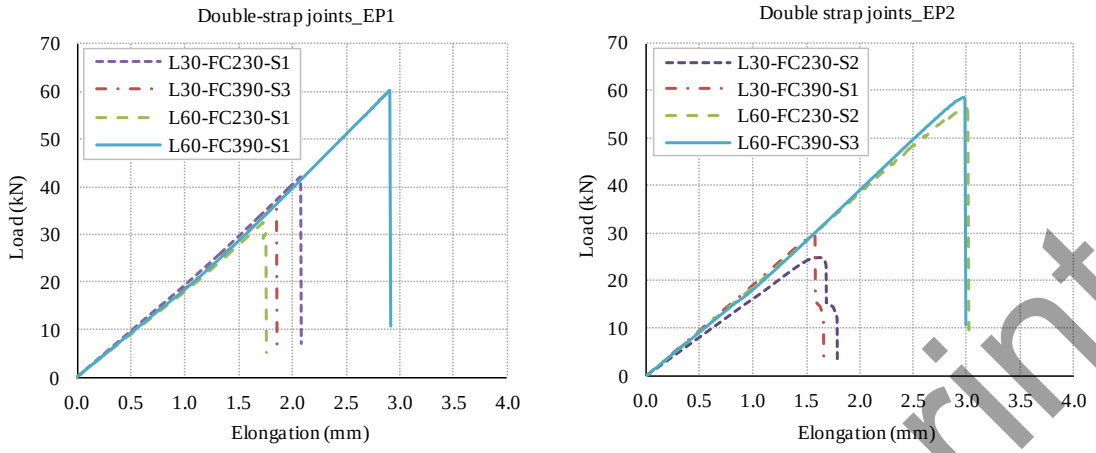

a) Adhesive EP1 b) Adhesive EP2

Fig. 5. *Load P [kN] - elongation δ [mm]* curves during the CFRP-steel double-strap joint tests (only instrumented specimens are shown).

3.1 Failure modes

In the present work, it is generally observed that the failure mode did not depend on the type of carbon fibre used nor the type of adhesive, but the bond length. In the case of short bond lengths $L_1 = 30$ *mm*, the failure mode was always produced by the separation of the adhesive layer from the steel surface, so that an adhesive failure mode in the steel-adhesive interface was observed (Fig. 6a).

L30-EP1-FC230-S3 L30-EP2-FC230-S1

a) $L_1 = 30$ *mm*

L60-EP1-FC230-S3 L60-EP2-FC230-S1

b) $L_1 = 60$ *mm*

Fig. 6. Failure modes of the test specimens with different bond lengths.

In the case of bond lengths $L_1 = 60$ *mm* (Fig. 6b), a mixed failure mode was reported: the failure occurred partly due to an adhesive failure mode (steel-adhesive interface and CFRP-adhesive interface), and partly

due to a cohesive failure mode (adhesive breaks). Failure mode of each specimen tested is reported in Table 4 and Table 5.

4. Design model calibration

For the adoption of a proper model to predict the strength of double-strap joints, the failure mode must be analysed. As previously discussed, authors consider that strain-based models (e.g Hart-Smith model [22]) are not convenient when failure mode is adhesive (failure at adhesive-steel interface), which was observed in specimens with $L_1 = 30$ *mm* in the present study. Also, for specimens with $L_1 = 60$ *mm* and adhesive EP2, the ductile behaviour of the adhesive was not fully developed, so plastic shear strains were not attained and the parameter γ_p in Hart-Smith model could not be determined.

Consequently, a fracture energy-based model was found more suitable to predict the debonding strength of double-strap joints with short bond lengths with adhesive failure mode. This approach is based on the ultimate energy that the adhesive joint can absorb during failure by cracking. In this sense, the interfacial fracture energy in shear G_{II} associated with the propagation of a crack in the adhesive layer (or at the interface between adherents, or a combination of both) is used to characterise the strength of the joint. When debonding starts from the gap between the steel plates (as in the specimens of this study) an estimation of the failure load $P_{u,theo}$ may be [36]:

$$P_{u,theo} = \alpha \frac{2}{\delta} \sqrt{E_s A_s b_a G_{II} (\delta + 1)} \quad (1)$$

Where δ is a measure of the stiffness unbalance between adherents:

$$\delta = \frac{E_s A_s}{2 E_f A_f} \quad (2)$$

E_s and A_s are the elastic modulus and the cross-section area of the steel plates, respectively; E_f and A_f are the elastic modulus and the cross-section area of the CFRP laminates, respectively; b_a is the width of the adhesive layer; and the corrector factor α is inserted in order to take account of the real bond length L_1 of the adhesive joint [36]:

$$\alpha = 1 - e^{-\lambda L_1}, \text{ with } \lambda = \sqrt{\frac{G_a}{t_a} \left(\frac{1}{E_f t_f} + \frac{2}{E_s t_s} \right)} \quad (3)$$

Where G_a is the shear modulus of the adhesive. The definition of a reliable strength model for the adhesive joint is fundamental for the estimation of the CFRP strengthening effectiveness in a steel structural element. Based on the results of this experimental campaign, an expression for the parameter that characterizes the shear behaviour of the joint, the interfacial fracture energy in shear G_{II}, was calibrated until the theoretical strength of the joint $P_{u,\,theo}$, from the fracture mechanics model in Eq. (1),

was adjusted to the experimental value obtained from test ($P_{u,\,theo} / P_{u,\,test} \approx 1$). The value of this parameter G_{II} for each specimen tested is shown in Table 4 and Table 5.

In previous research works [35, 37] the interfacial fracture energy G_{II} in shear (pure mode II) in double-strap joint tests was found to be related to the thickness t_a of the adhesive and also to mechanical parameters of the adhesive, such as the tensile strain energy R_a (area under the uni-axial tensile stress-strain curve), the tensile strength $f_{t,a}$ or the shear modulus G_a. Also, some authors [36] indicate that the maximum transferable load is a function of the adhesive thickness. In the present work, it was considered that the parameter R_a can be the most representative of the mechanical behaviour of the adhesive in terms of ductility and energy accumulation until failure, so this parameter was adopted for the analytical model instead of the tensile strength $f_{t,a}$. As well as in previous research works, different CFRP laminates were tested in the present study, so the axial stiffness of the CFRP laminate $K_f = A_f E_f$ was also included. For relatively short bond lengths, fracture mechanics analytical models overestimate the failure load of bonded interfaces [38]. As the bond lengths L_1 were presumably shorter or around the effective bond length L_e, authors considered including the parameter L_1/L_e (relation between bond length and theoretical effective bond length) in the empirical expression for the interfacial fracture energy G_{II} calibrated in this work. In this way, for short bond lengths (typically with $L_1/L_e < 1$), the interfacial fracture energy G_{II} for bond lengths $L_1 < L_e$ could be reduced. A nonlinear function relating the interfacial fracture energy and the parameters mentioned above was chosen to approximate the test data, with the unknown coefficients *A*, *B*, *C* and *D* of this function varied to minimise the errors between the theoretical predictions $P_{u,\,theo}$ and the test results $P_{u,\,test}$. This process led to an expression in the form:

$$G_{II} = A \left(\frac{L_1}{L_e}\right) t_a^{\,B} R_a^{\,C} K_f^{\,D} \quad (N/mm^2 \cdot mm) \tag{4}$$

Where, according to [36]:

$$L_e = \frac{5}{\lambda} \quad (mm) \tag{5}$$

4.1 Database

In order to have a higher number of experimental results to adjust the parameters of the proposed analytical model, a large database (115 tests) was created (see Annex 1) with results of double-strap joints tests consulted in the literature [23, 24, 27, 28, 36]. Specimens from database have similar geometries and configurations comparable to the tests performed in the present work (only specimens with short bond lengths under $L_1 = 80$ *mm* are considered). The aim is to develop a model that includes not only the results obtained in the present experimental campaign, but also the results from tests performed by other authors. The following best-fit equation is proposed to predict G_{II} based on the test results from this database, including the results of the present study:

$$G_{II} = 0.1 \left(\frac{L_1}{L_e}\right) \sqrt[3]{(t_a R_a)^2}\, K_f^{\,1/4} \quad (N/mm^2 \cdot mm) \tag{6}$$

It is important to note that this expression is valid for joints with an adequate surface preparation of the steel (such as grit blasting) that fail in a cohesive or adhesive mode. This means that the strength prediction in specimens with no proper surface preparation or different failure modes (delamination/rupture of CFRP, steel yielding, etc.) may not fit precisely this expression.

This explicit formula provides a method to predict the average bond strength of CFRP-steel double-strap joint specimens with short bond lengths, including a range of values for CFRP plate and adhesive properties commonly available, as shown in Table 6. As it can be seen in Fig. 7, the above expression provides acceptable predictions of the experimental failure loads of the specimens not only of the present work, but also of the data base considered, with a coefficient of determination $R^2 = 0.82$.

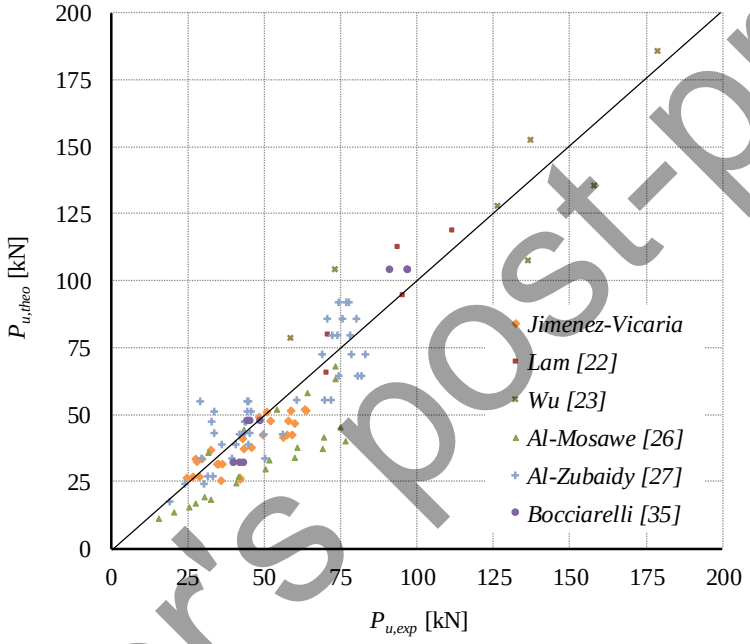

Fig. 7. Comparison between test and predicted ultimate loads (115 tests)

Table 6. Range of values in the main parameters of the CFRP-steel double-strap joint tests used to calibrate the model.

	L_1	t_a	R_a	K_f	b_s	t_s	b_f	t_f	E_f	E_a
	mm	mm	MPa mm/mm	N	mm	mm	mm	mm	N/mm^2	N/mm^2
Min	10	0.34	0.068	1.9E+06	30	5	10	0.17	76652	1451
Max	80	2.16	0.433	3.5E+07	60	20	60	3.66	478730	4951

For design purposes, the coefficients A, B, C and D in Eq. (4) were recalculated to obtain a formula that can predict the characteristic bond strength of double-strap joints. This characteristic value is usually considered as the 95 percentile of the probability distribution of the test data, which means that 95 % of the experimental results lie above this value. Assuming normality of joint strength data, the characteristic

values were obtained by using the same data fitting method as for Eq. (6), but the experimental debonding load was substituted by this experimental value minus 1.645 times the standard deviation of specimens with the same CFRP, adhesive and bonded area. In Fig. 8, both the predictions of the average and characteristic (95 %) bond strength are plotted against the experimental failure loads. The following best-fit equation is proposed to predict G_{II} to be used in the design expression for joint strength in Eq. (1):

$$G_{II} = 0.03 \left(\frac{L_1}{L_e}\right) (t_a R_a)^{0.9} K_f^{0.34} \quad (N/mm^2 \cdot mm) \tag{7}$$

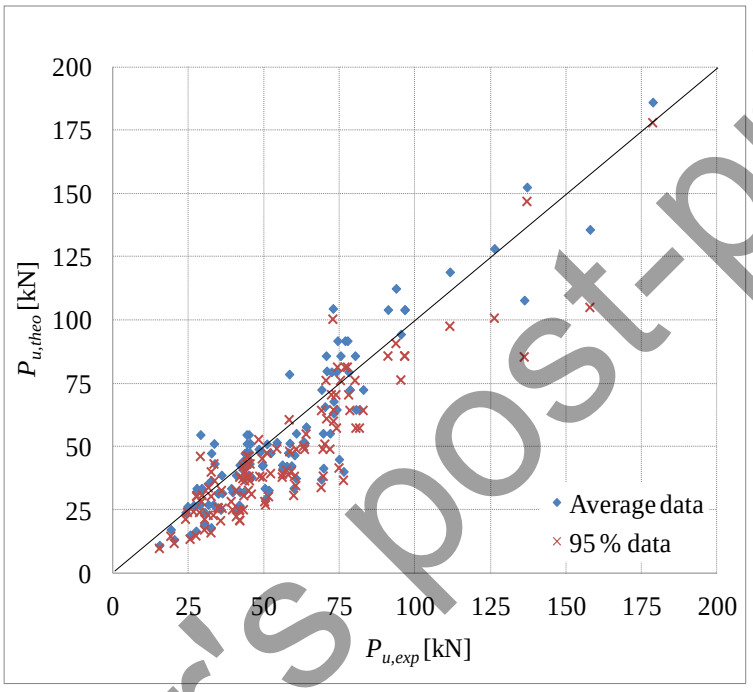

Fig. 8. Comparison between average and characteristic predicted bond strength

5. Numerical simulation

Analytical models can provide a good overall measure of joint strength in simple geometries and simple loading conditions (as the one of these double-strap joint tests). But these analytical models are not able to provide detailed information in the regions of high stresses where failure initiation occurs, especially when complex geometries and loading conditions are used. Authors consider interesting to validate that numerical models of the adhesive joints based on cohesive elements could be used for the prediction of bond strength in more complex joints.

Using Abaqus finite element software, the double-strap joint specimens were simulated using cohesive zone models (CZM) for the adhesive layers, which are common in literature for the simulation of adhesive bonds [39, 40, 41]. In the present work, a continuum-based approach, i.e. using the cohesive elements to model solids rather interfaces, was considered to model the finite thickness of the adhesive layer. In this case, three-dimensional continuous elements C3D8R were used for the modelling of the adherents (steel plates and CFRP laminates), with an elastic behaviour with the mechanical properties

previously described (the steel plates are simulated with a linear-elastic behaviour since the maximum stresses in the steel are below yielding in all cases during testing). For the adhesive layer, COH3D8 cohesive elements were used, with a behaviour governed by a traction-separation law, and with the following parameters to be introduced in the model: interfacial stiffness (pre-damage behaviour), maximum stresses before damage (criterion of damage initiation) and the damage evolution law in the cohesive zone. The strength predictions of CZM modelling were expected to be mesh independent, as demonstrated in previous research works [42].

The FEM meshes were built with horizontal symmetry (XZ plane) to reduce the total number of elements. Restraining and loading conditions were introduced to faithfully model the real testing conditions, consisting on clamping of the joint at one end and applying a tensile load at the opposite end (Fig. 9). The meshes were constructed taking advantage of the automatic meshing algorithms of ABAQUS®, from a manual seeding procedure that includes biasing towards the overlap edges, since these theoretically singular regions show large stress gradients, thus allowing to accurately capture these phenomena.

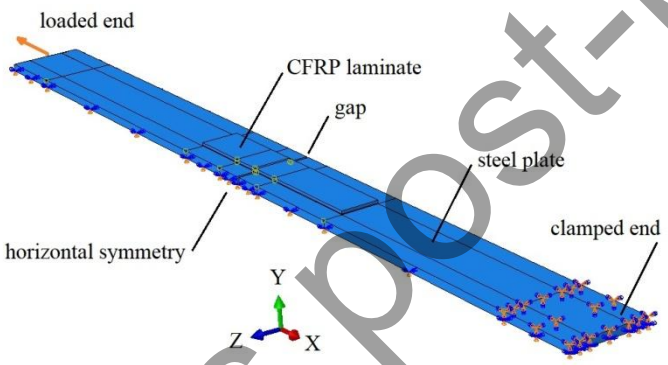

Fig. 9. 3D view of FEM model of the double-strap joint ($L_1 = 60$ *mm*).

The traction-separation law assumes an initial linear elastic behaviour, and the stiffness parameters of the adhesive layer are given by K_{nn}, K_{ss} and K_{tt}. A suitable approximation for thin adhesive layers is provided with $K_{nn} = E$, $K_{ss} = G$, $K_{tt} = G$, being E and G the longitudinal and transverse elastic moduli of the adhesive, respectively [42]. For the initiation of damage, the quadratic nominal stress criterion (*Quads damage* in ABAQUS®) was considered, as it is shown to give accurate results in previous works [43]. The criterion is expressed as:

$$\left\{ \frac{\langle t_n \rangle}{t_n^0} \right\}^2 + \left\{ \frac{t_s}{t_s^0} \right\}^2 + \left\{ \frac{t_t}{t_t^0} \right\}^2 = 1 \qquad (8)$$

where t_n, t_s and t_t represent the pure mode nominal stresses (mode-I, mode-II and mode-III, respectively), and t_n^0, t_s^0 and t_t^0 represent the corresponding pure mode nominal strengths. ‹› are the Macaulay brackets, indicating that damage is not initiated by a purely compressive stress state. Since the values of the interface mode-I and mode-III strengths t_n^0 and t_t^0 have a negligible influence on the numerical results in double-strap joints (mode-II governs), the same value adopted for t_s^0 was assumed for these parameters.

As an approximation, the pure mode-II nominal shear strength t_s^0 to use in the model was selected based on the tensile strength of the adhesive, $t_s^0 = 30\ MPa$ for EP1 and $t_s^0 = 19\ MPa$ for EP2.

The material stiffness is degraded under a linear softening law, and complete separation is predicted by the critical fracture energy required for pure mode-II failure, which is equal to the area under the traction–separation law (Fig. 10). The values of critical fracture energy used in the numerical models were those predicted by the model calibrated in the present work, G_{II} (Table 4 and Table 5). In this way, the analytical model (calibrated from experimental results) was compared with the numerical results to validate their suitability for failure load prediction. Table 7 shows the values introduced in ABAQUS® for the simulation of the traction-separation law in the adhesive layers (specimens L30-EP1-FC230 and L60-EP2-FC390 are considered).

Table 7. Parameters of the traction-separation behaviour for the cohesive elements to model adhesive layer.

	interfacial stiffness			*damage initiation*			*damage evolution*
	K_{nn} (N/mm^3)	K_{ss} (N/mm^3)	K_{tt} (N/mm^3)	t_n^0 (N/mm^2)	t_s^0 (N/mm^2)	t_t^0 (N/mm^2)	G_{II} (N/mm)
L30-EP1-FC230	4951	1834	1834	30.0	30.0	30.0	0.56
L60-EP2-FC390	1451	537	537	19.0	19.0	19.0	1.40

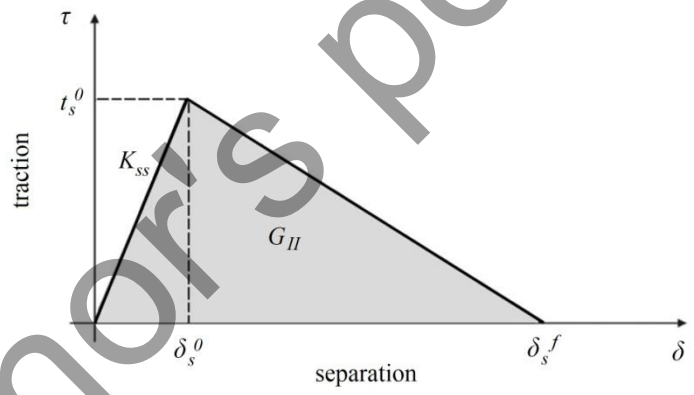

Fig. 10. Traction–separation law with linear softening available in ABAQUS® (for pure mode-II).

In the numerical model, fracture took place in the adhesive layer, first at the joint gap between the steel plates, and then propagating quickly (brittle failure) towards the CFRP end of the shortest bond lengths L_1, as shown experimentally. Complete damage was attained in a cohesive element of the adhesive layer when the parameter SDEG (corresponding to the stiffness degradation) equalled 1.0, as seen in the examples of Fig. 11 and Fig. 12 for specimens L30-EP1-FC230 and L60-EP2-FC390 (specimens with the highest experimental failure load for each bond length L_1). While the parameter $SDEG = 0$, the material is undamaged, and more load can be sustained. A numerical model was carried out for each combination of parameters (bond length L_1, carbon fibre and adhesive), modelling the specimens monitored with strain gauges during experimental tests, and the failure loads were obtained (Table 4 and Table 5). The results were close to those computed from the analytical model for specimens with $L_1 = 60\ mm$ (the maximum

difference is 7 % in specimen L60-EP2-FC390). For specimens with $L_1 = 30$ *mm* the biggest difference was obtained (34 % in specimen L30-EP2-FC390), so for bond lengths $L_1 = 30$ *mm* the numerical model did not fit the analytical predictions. This may be attributed to the use of an imprecise value of K_{ss} (shear modulus G_a) of the adhesive in the numerical model, which in the case of short bond lengths $L_1 = 30$ *mm* may be the decisive parameter, instead of the interfacial fracture energy G_{II} in shear.

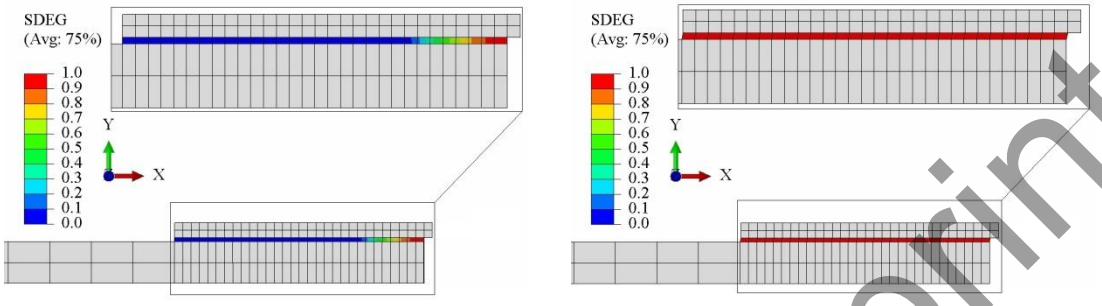

a) Damage initiation near the joint gap b) Propagation to the CFRP end

Fig. 11. Progressive failure in the adhesive layer for specimen L30-EP1-FC230 using CZMs.

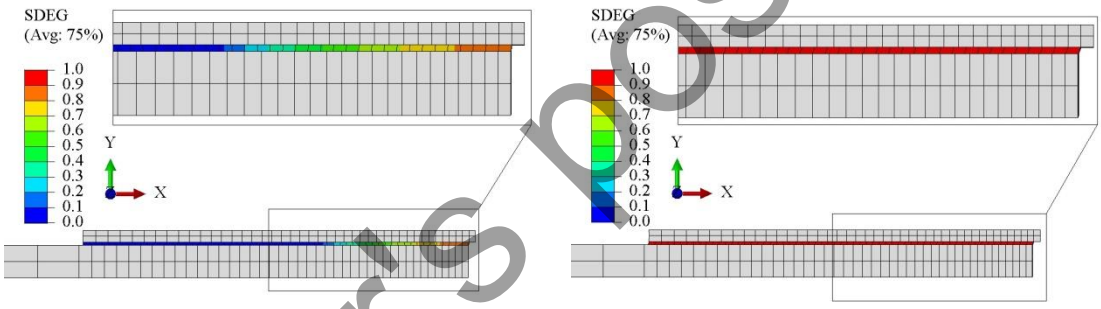

a) Damage initiation near the joint gap b) Propagation to the CFRP end

Fig. 12. Progressive failure in the adhesive layer for specimen L60-EP2-FC390 using CZMs.

The *load P [kN] - elongation δ [mm]* curves obtained from the numerical models are presented for the specimens with $L_1 = 60$ *mm* in Fig. 13, being the elongation the longitudinal displacement of the specimen end where the load was applied in the model. It is observed that the slope of the curves was slightly higher for specimens with stiffer carbon fibre (FC390), and this was more pronounced in specimens with ductile adhesive EP2. Also, elongation at failure was higher for specimens with ductile adhesive EP2. At damage initiation near the joint gap (first cohesive elements reach SDEG = 1) a change in the slope of the load-elongation curve was observed (points A in Fig. 13). When damage propagated to the CFRP end (all cohesive elements in the joint had SDEG = 1) there was a sudden drop in the load (points B in Fig. 13), and the joint failure was attained.

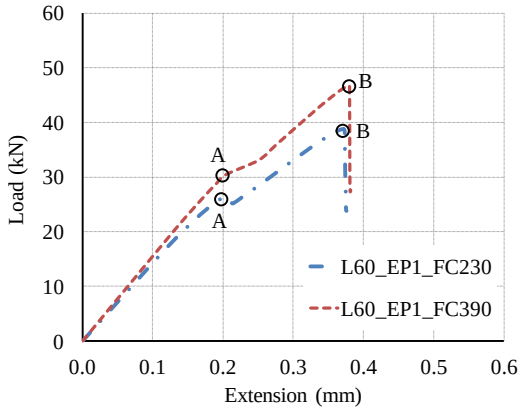

a) Adhesive EP1

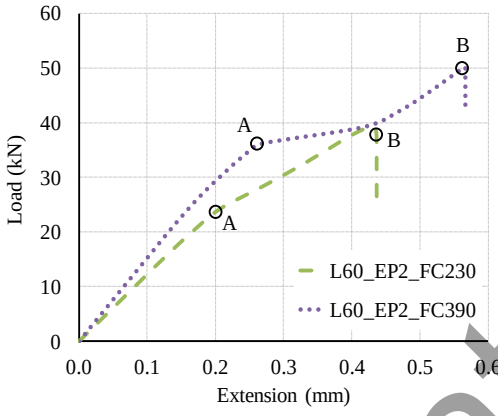

b) Adhesive EP2

Fig. 13. *Load P [kN] - elongation δ [mm]* curves from the numerical models of L_1 = *60 mm* CFRP-steel double-strap joints.

As an example, the results obtained for the numerical model of the specimens L30-EP1-FC230 and L60-EP2-FC390 are shown in Fig. 14 and Fig. 15, respectively, where the failure load $P_{u,\,num}$ = *19.24 kN* and $P_{u,\,num}$ = *45.28 kN* were obtained in each case. It must be considered that the value shown in the figure, in Newtons, should be doubled as the model represents the half of the specimen due to the symmetry applied. Also the values of the parameter SDEG in the adhesive layer and the stresses in the CFRP in the longitudinal direction S11 (in MPa) are represented for these loads. A more detailed study on the distribution of longitudinal stresses S11 in the CFRP laminates is presented in the next section.

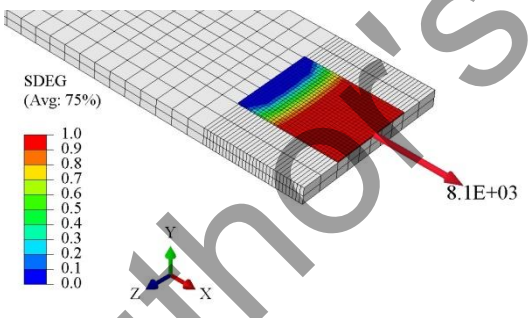

a) Stiffness degradation (SDEG) of the adhesive layer

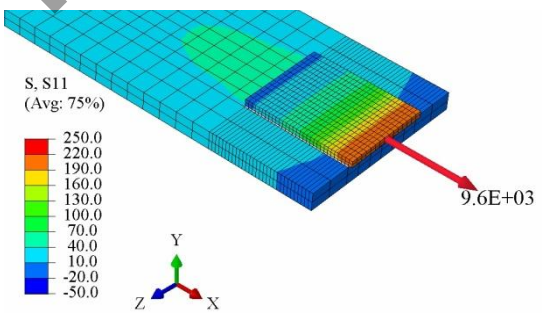

b) Longitudinal stresses S11 (in MPa) at failure load

Fig. 14. Numerical model of the specimen L30-EP1-FC230.

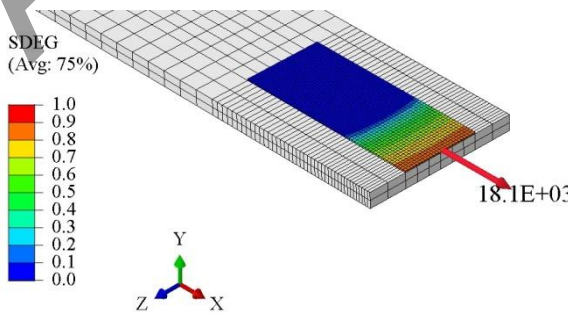

a) Stiffness degradation (SDEG) of the adhesive layer

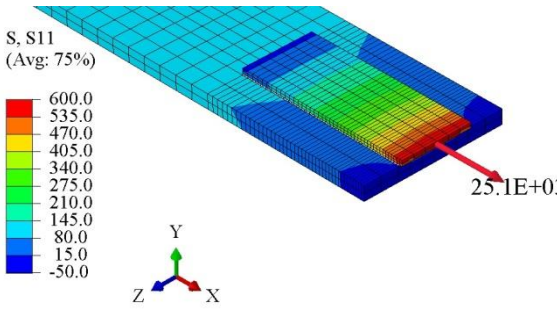

b) Longitudinal stresses S11 (in MPa) at failure load

Fig. 15. Numerical model of the specimen L60-EP2-FC390.

5.1 *Stress distribution in the CFRP*

For each combination of parameters (bond length, adhesive and CFRP), one specimen (indicated in Table 4 and Table 5) was instrumented by strain gauges attached to the CFRP to measure the strains in the CFRP laminates during testing. The gauges were placed in the centre of the specimen (in correspondence with the joint, gauge G3), and symmetrically at a distance of $L_1/2$ from the joint (gauges G2 and G4), as shown in Fig. 16. The measured strains were multiplied by the modulus of elasticity of the CFRP laminate to compute the corresponding stresses, which are then compared with those obtained in the numerical models. The strain monitoring points in the numerical models were selected as close as possible to the experimental locations where the strain gauges were placed, and at the top face of the CFRP laminates, where strain gauges were attached. In Fig. 17, for different load levels (until failure load in numerical models), the experimental stresses are compared with the stresses obtained in the FEM.

Also, the stresses S11 along the centreline of the CFRP laminate in the numerical models are compared to the stresses measured experimentally, at the maximum load obtained in the FEM. It can be seen in Fig. 18a-d that the numerical models simulate the stress distributions along the centreline of the CFRP laminate reasonably well, especially for specimens with $L_1 = 60$ *mm*. However, it is evident that there is a pronounced difference between the predicted and measured stress values at the joint location (G3) for specimens with stiffer adhesive EP1 and carbon fibre FC390.

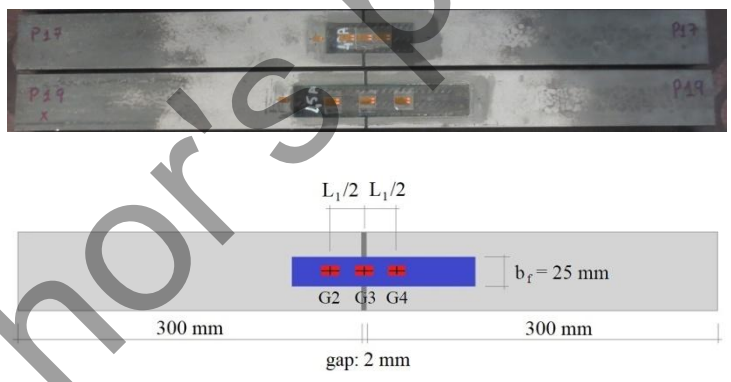

Fig. 16. Instrumented specimens with strain gauges on the CFRP laminates.

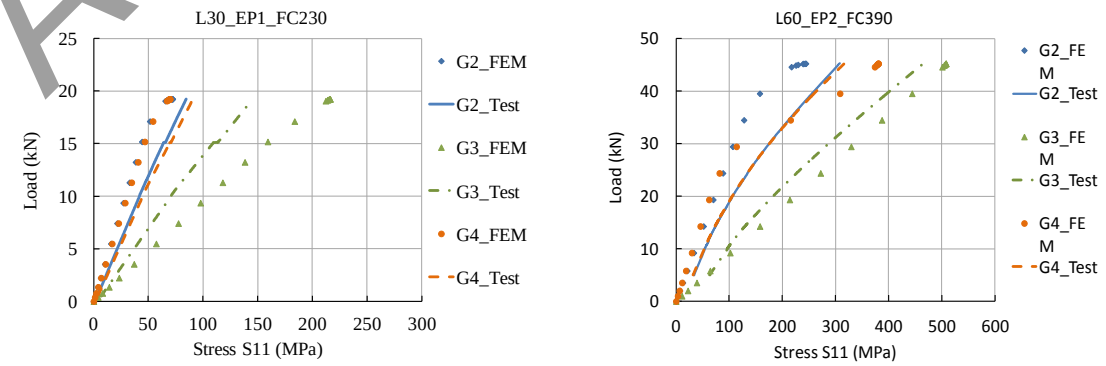

a) L30-EP1-FC230 b) L60-EP2-FC390

Fig. 17. Comparison of numerical model and test load versus axial stress in CFRP plates for the test specimens L30-EP1-FC230 and L60-EP2-FC390.

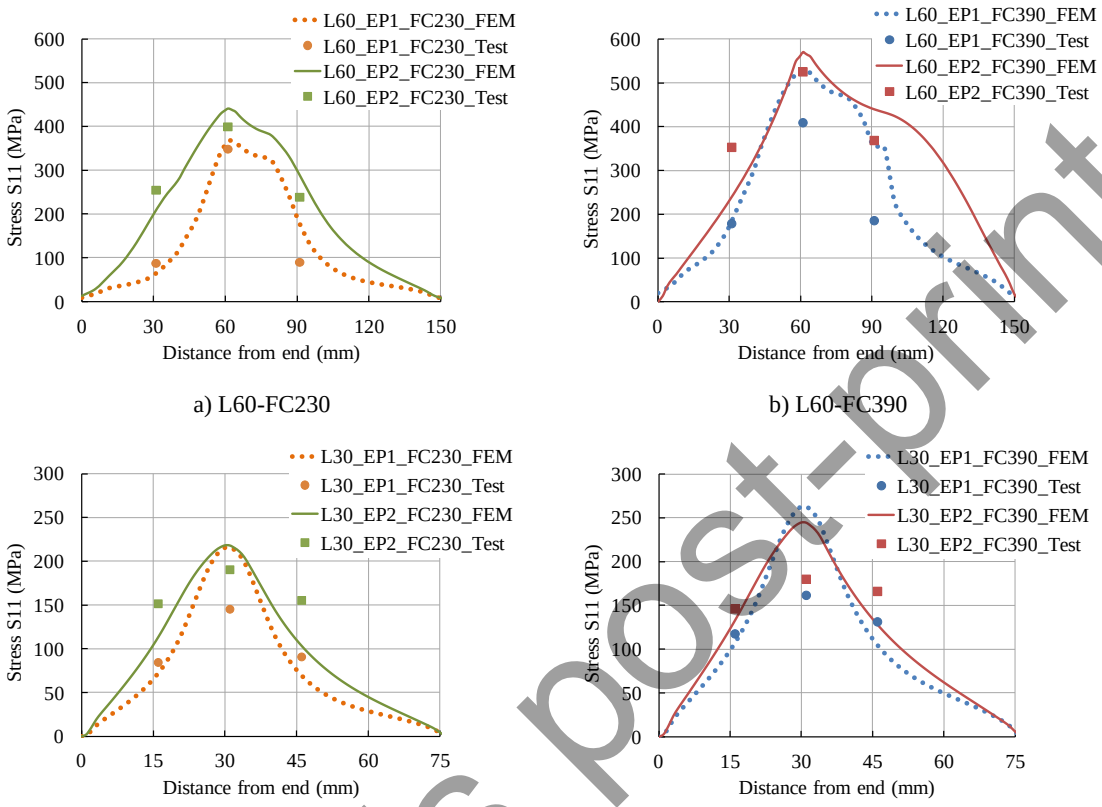

a) L60-FC230 b) L60-FC390

c) L30-FC230 d) L30-FC390

Fig. 18. Numerical model and test axial stress S11 in CFRP plates at maximum load.

6. Conclusions

From the work presented in this paper, the following conclusions can be derived:

The highest experimental joint strength (P_{max} = *63.63 kN*) was obtained for bond length L_1 = *60 mm* using ductile adhesive EP2 and stiffer carbon fibre FC390. However, when using EP2 adhesive, the joint strength was hardly increased by using a stiffer carbon fibre (FC 390) compared to FC230. This could be probably because the effective bond length L_e was expected to be higher than L_1 = *60 mm*, so the ductile behaviour of adhesive EP2 was not fully developed and the potential maximum strength of the joint was not attained.

When using adhesive EP1 (fragile adhesive), it is convenient to use a stiffer carbon fibre (FC390) in the case of bond length L_1 = *60 mm*, not being so for shorter bond lengths L_1 = *30 mm*. In case short bond lengths L_1 = *30 mm* must be used, the highest strengths were obtained with adhesive EP1 and carbon fibre FC230 (less stiff fibre), with 49 % higher failure load compared to that obtained with the same carbon fibre (FC230) and ductile adhesive (EP2).

The available length to bond the CFRP patches to strengthen the metallic element will motivate the selection of the best combination of carbon fibre and adhesive to obtain the highest joint strength. Based on experimental results, for the shortest bond lengths tested ($L_1 = 30\ mm$) it is better to use EP1 adhesive with FC230 carbon fibre, while for bond lengths $L_1 = 60\ mm$ EP2 adhesive with FC390 carbon fibre could be more efficient.

In the present work, it is generally observed that the failure mode did not depend on the type of carbon fibre used nor the type of adhesive, but the bond length. The failure mode was adhesive (failure in the steel-adhesive interface) for $L_1 = 30\ mm$, and a mixed adhesive-cohesive failure mode for $L_1 = 60\ mm$.

An explicit formula to predict the bond strength of CFRP-steel double-strap joint specimens with short bond lengths was calibrated based on experimental results from a large database, including the tests of the present work. This model is based on interfacial fracture energy in shear G_{II}, which is related to the thickness and tensile strain energy of adhesive layer, the axial stiffness of the CFRP laminate and the bond length.

The results from the numerical models were close to those computed from the analytical model for specimens with $L_1 = 60\ mm$ (the maximum difference was 7 % in specimen L60-EP2-FC390). For specimens with shorter bond lengths $L_1 = 30\ mm$ the biggest difference was obtained (34 % in specimen L30-EP2-FC390), so in this case ($L_1 = 30\ mm$) the CZM developed did not fit the analytical predictions.

Numerical models simulated the stress distributions along the centreline of the CFRP laminate reasonably well, especially for specimens with $L_1 = 60\ mm$. However, there was a pronounced difference between the predicted and measured stress values at the joint location (G3) for specimens with the shortest bond lengths tested $L_1 = 30\ mm$. This may be attributed to the use of an imprecise value of K_{ss} (shear modulus G_a) of the adhesive in the numerical model, which in this case of bond lengths $L_1 = 30\ mm$ may be the control parameter.

Acknowledgements

The research leading to these results has received partial funding from the European Union's Horizon 2020 Programme in the framework of the research project IN2TRACK under grant agreement n° 730841. The authors also wish to thank the laboratory technicians of ACCIONA Construction Technological Centre, where all the tests were carried out.

References

1 Hosseini A., Ghafoori E., Al-Mahaidi R., Zhao X.L., Motavalli M. Strengthening of a 19th-century roadway metallic bridge using nonprestressed bonded and prestressed unbonded CFRP plates, Construction and Building Materials 209 (2019) 240–259.

2 Ghafoori E., Motavalli M., Nussbaumer A., Herwig A., Prinz G.S., Fontana M. Design criterion for fatigue strengthening of riveted beams in a 120-year-old railway metallic bridge using pre-stressed CFRP plates. Composites Part B, 2015. 68: p. 1-13.

3 Teng, J.G., Yu, T., and Fernando, D. 2012. Strengthening of steel structures with FRP composites. Journal of Constructional Steel Research, 78, 131-143.

4 Robert J. Dexter and Justin M. Ocel. Manual for repair and retrofit of fatigue cracks in steel bridges. FHWA Publication No. FHWA-IF-13-020. March 2013.

5 Mohammad Ali Saeimi Sadigh. Creep simulation of adhesively bonded joints using modified generalized time hardening model. Journal of Mechanical Science and Technology 30(4):1555-1561, April 2016.

6 Arash Reza; Mohammad Shishesaz; Khosro Naderan-Tahan. The effect of viscoelasticity on creep behavior of double-lap adhesively bonded joints. Latin American Journal of Solids and Structures, vol.11 no.1 Rio de Janeiro Jan. 2014.

7 Fawzia, S. 2013. Evaluation of shear stress and slip relationship of composite lap joints. Composite Structures, 100, pp. 548-553.

8 Yu, T., Fernando, D., Teng, J.G., and Zhao, X.L. 2012. Experimental study on CFRP-to-steel bonded interfaces. Composites Part B: Engineering, 43(5), 2279-2289.

9 Y. Yu, Static and Cyclic Behavior of Steel Beams Retrofitted with Fiber Reinforced Polymer Laminates PhD thesis, Nanyang Technological University, Singapore, 2008.

10 M. Bocciarelli, P. Colombi, G. Fava, C. Poggi, Interaction of interface delamination and plasticity in tensile steel members reinforced by CFRP plates, Int. J. Fract. 146 (2007) 79–92.

11 Colombi, P. and Poggi, C. 2006. Strengthening of tensile steel members and bolted joints using adhesively bonded CFRP plates. Construction and Building Materials, 20 (1-2), pp. 22-33.

12 Al-Mosawe, A., Al-Mahaidi, R. and Zhao, X.L. 2016. Bond behaviour between CFRP laminates and steel members under different loading rates. Composite Structures, 148, pp. 236-251

13 Y.J. Kim, J. LaBere, I. Yoshitake, Hybrid epoxy-silyl modified polymer adhesives for CFRP sheets bonded to a steel substrate, Compos. Part B 51 (2013) 233–245.

14 S.P. Chiew, Y. Yu, C.K. Lee, Bond failure of steel beams strengthened with FRP laminates – Part 1: Model development, Compos. Part B 42 (2011) 1114–1121.

15 H.B. Liu, X.L. Zhao, R. Al-Mahaidi, Effect of fatigue loading on bond strength between CFRP sheets and steel plates, Int. J. Struct. Stab. Dyn. 10 (2010) 1–20.

16 Fawzia, S., Zhao, X.L., and Al-Mahaidi, R. 2010. Bond-slip models for double strap joints strengthened by CFRP. Composite Structures, 92(9), pp. 2137-2145.

17 Fawzia, S., Al-Mahaidi, R., and Zhao, X.L. 2006. Experimental and finite element analysis of a double strap joint between steel plates and normal modulus CFRP. Composite Structures, 75(1-4), 156-162.

18 Xiao-Ling Zhao and Lei Zhang. 2007. State-of-the-art review on FRP strengthened steel structures. Engineering Structures, 29, 1808–1823.

19 Adams RD, Mallick V. A method for the stress analysis of lap joints. The Journal of Adhesion 1992;38(3-4):199-217.

20 Silva, L.F.M.; Neves, P.; Adams, R.; Wang, A. and Spelt, J. (2009). Analytical models of adhesively bonded joints-Part II: Comparative study. International Journal of Adhesion and Adhesives, 29(3):331-341.

21 Raul D. S. G. Campilho. Strength Prediction of Adhesively-Bonded Joints. CRC Press. 2017.

22 Hart-Smith L. Adhesive-bonded double-lap joints. In: Technical report, National Aeronautics and Space Administration CR-112235: Washington DC, USA; 1973.

23 A. Lam, J.J.R. Cheng, M.C.H. Yam, G.D. Kennedy, Repair of steel structures by bonded carbon fiber reinforced polymer patching: experimental and numerical study of carbon fiber reinforced polymer, Can. J. Civ. Eng. 34. (2007) 1542–1553.

24 Wu, C., Zhao, X.L., Duan, W.H. and Al-Mahaidi, R. Bond characteristics between ultra-high modulus CFRP laminates and steel, Thin-Walled Structures, 51 (2012), 147–157.

25 Fawzia, S., Zhao, X.L., Al-Mahaidi, R. and Rizkalla, S. 2005. Bond characteristics between CFRP and steel plates in double strap joints. Advanced Steel Construction, 1(2), pp. 17-27.

26 Peiris, N. 2011. Steel beams strengthened with Ultra High Modulus CFRP laminates. PhD thesis, College of Engineering at the University of Kentucky, Lexington, Kentucky.

27 Al-Mosawe, A., Al-Mahaidi, R. and Zhao, X.L. Effect of CFRP properties on the bond characteristics between steel and CFRP laminate under quasi-static loading, Construction and Building Materials, 98 (2015), 489–501.

28 H. Al-Zubaidy, R. Al-Mahaidi, X.L. Zhao, Experimental investigation of bond characteristics between CFRP fabrics and steel plate joints under impact tensile loads, Compos. Struct. 94 (2012) 510–518.

29 Fernando, D., Yu, T. and Teng, J. G. 2014. Behavior of CFRP Laminates Bonded to a Steel Substrate Using a Ductile Adhesive, Journal of Composites for Construction, 18(2), 04013040.

30 Schnerch, D., Dawood, M., Rizkalla, S., Sumner, E. and Stanford, K. 2006. Bond behavior of CFRP Strengthened Steel Structures. Advances in Structural Engineering, 9 (6), 805-817.

31 Jimenez-Vicaria, J. David, G. Pulido, M. Dolores and Castro-Fresno, Daniel. Evaluation of the bond behaviour in CFRP-steel double-strap joints. In: Proceedings of the 7th Euro-American Congress on Construction Pathology, Rehabilitation Technology and Heritage Management, REHABEND 2018, Caceres, Spain.

32 Fernando, D., Teng, J. G., Yu, T. and Zhao, X. L. 2013. Preparation and Characterization of Steel Surfaces for Adhesive Bonding. Journal of Composites for Construction, 17(6), 04013012.

33 ASTM D3039/D3039M-17. Standard Test Method for Tensile Properties of Polymer Matrix Composite Materials.

34 ASTM D 638-14. Standard Test Method for Tensile Properties of Plastics.

35 Xia, S.H., and Teng, J.G. 2005. Behavior of FRP-to-steel bond joints. In Proceedings of International Symposium on Bond Behaviour of FRP in Structures (BBFS 2005), Hong Kong, December, pp. 419-426.

36 M. Bocciarelli, P. Colombi, G. Fava, C. Poggi, Prediction of debonding strength of tensile steel/CFRP joints using fracture mechanics and stress based criteria, Eng. Frac. Mech. 76 (2009) 299-313.

37 Fernando ND. Bond behaviour and debonding failures in CFRP-strengthened steel members. PhD Thesis, The Hong Kong Polytechnic University. Hong Kong, China; 2010.

38 P. Cornetti, V. Mantič, A. Carpinteri. Finite Fracture Mechanics at elastic interfaces. International Journal of Solids and Structures. Volume 49, Issues 7–8, April 2012, Pages 1022-1032.

39 Baltasar Pérez, N. Análisis mediante elementos finitos de uniones adhesivas en materiales metálicos y compuestos. Universidad Politécnica de Valencia, Escuela Técnica Superior de Ingeniería del Diseño. Septiembre 2016.

40 Teng, J.G., Fernando, D. and Yu, T. 2015. Finite element modelling of debonding failures in steel beams flexurally strengthened with CFRP laminates. Engineering Structures, 86, 213-224.

41 De Lorenzis, L., Fernando, D., and Teng, J.G. 2013. Coupled mixed-mode cohesive zone modeling of interfacial stresses in plated beams. International Journal of Solids and Structures, 50 (14-15), 2477-2494.

42 R.D.S.G. Campilho, M.D. Banea, A.M.G. Pinto, L.F.M. da Silva, A.M.P. de Jesus. Strength prediction of single- and double-lap joints by standard and extended finite element modelling. International Journal of Adhesion & Adhesives 31 (2011) 363–372.

43 R.D.S.G. Campilho, de Moura MFSF, Pinto AMG, Morais JJL, Domingues JJMS. Modelling the tensile fracture behaviour of CFRP scarf repairs. Composites: Part B-Engineering 2009; 40: 149-57.

652

Annex 1. Database

											Average		Design		
Specimen	b_s mm	t_s mm	b_f mm	t_f mm	E_f N/mm^2	t_a mm	G_a N/mm^2	R_a Mpa	L_1 mm	L_e mm	G_{theo} N/mm	$P_{u,theo}$ N	G_{theo} N/mm	$P_{u,theo}$ N	$P_{u,exp}$ kN
Jimenez-Vicaria															
L30-EP1-FC230-S1	50.0	10.0	25.0	1.92	117146	0.67	1834	0.09	30	41	0.56	25.83	0.36	20.58	42.18
L30-EP1-FC230-S2	50.0	10.0	25.0	1.98	117146	0.65	1834	0.09	30	41	0.56	26.15	0.35	20.79	42.10
L30-EP1-FC230-S3	50.0	10.0	25.0	1.74	117146	0.91	1834	0.09	30	46	0.60	24.98	0.41	20.54	35.81
L30-EP1-FC390-S1	50.0	10.0	25.0	1.91	183605	0.71	1834	0.09	30	50	0.53	31.48	0.36	25.76	34.81
L30-EP1-FC390-S2	50.0	10.0	25.0	1.90	183605	0.67	1834	0.09	30	49	0.53	31.39	0.35	25.51	35.07
L30-EP1-FC390-S3	50.0	10.0	25.0	1.91	183605	0.65	1834	0.09	30	48	0.53	31.46	0.34	25.48	36.34
L30-EP2-FC230-S1	50.0	10.0	25.0	1.84	117146	0.44	537	0.37	30	60	0.72	26.79	0.57	23.83	28.80
L30-EP2-FC230-S2	50.0	10.0	25.0	1.77	117146	0.54	537	0.37	30	66	0.75	26.21	0.62	23.84	24.85
L30-EP2-FC230-S3	50.0	10.0	25.0	1.83	117146	0.51	537	0.37	30	65	0.73	26.62	0.60	24.09	26.85
L30-EP2-FC390-S1	50.0	10.0	25.0	2.06	183605	0.50	537	0.37	30	80	0.68	33.04	0.58	30.61	29.67
L30-EP2-FC390-S2	50.0	10.0	25.0	2.05	183605	0.43	537	0.37	30	74	0.66	33.37	0.55	30.36	27.86
L30-EP2-FC390-S3	50.0	10.0	25.0	1.97	183605	0.53	537	0.37	30	81	0.69	32.27	0.60	30.03	27.88
L60-EP1-FC230-S1	50.0	10.0	25.0	1.70	117146	0.97	1834	0.09	60	47	1.22	36.46	0.83	30.17	32.67
L60-EP1-FC230-S2	50.0	10.0	25.0	1.78	117146	0.90	1834	0.09	60	46	1.19	37.03	0.81	30.43	43.51
L60-EP1-FC230-S3	50.0	10.0	25.0	1.85	117146	0.90	1834	0.09	60	47	1.19	37.69	0.80	31.03	46.02
L60-EP1-FC390-S1	50.0	10.0	25.0	1.89	183605	0.71	1834	0.09	60	50	1.07	46.50	0.71	38.03	60.24
L60-EP1-FC390-S2	50.0	10.0	25.0	1.97	183605	0.69	1834	0.09	60	50	1.06	47.39	0.70	38.70	58.18
L60-EP1-FC390-S3	50.0	10.0	25.0	1.93	183605	0.78	1834	0.09	60	53	1.08	47.33	0.74	39.17	52.35
L60-EP2-FC230-S1	50.0	10.0	25.0	1.80	117146	0.86	537	0.37	60	83	1.61	42.08	1.48	40.45	57.66
L60-EP2-FC230-S2	50.0	10.0	25.0	1.75	117146	0.75	537	0.37	60	77	1.58	41.32	1.41	39.03	56.33
L60-EP2-FC230-S3	50.0	10.0	25.0	1.85	117146	0.74	537	0.37	60	78	1.56	42.30	1.40	40.00	59.23
L60-EP2-FC390-S1	50.0	10.0	25.0	1.82	183605	0.66	537	0.37	60	88	1.44	51.23	1.30	48.75	63.63
L60-EP2-FC390-S2	50.0	10.0	25.0	1.86	183605	0.73	537	0.37	60	93	1.46	51.79	1.36	49.91	63.25
L60-EP2-FC390-S3	50.0	10.0	25.0	1.84	183605	0.56	537	0.37	60	81	1.40	51.24	1.22	47.85	58.66
L60-EP1-FC230-S1_2	50.0	10.0	25.0	1.93	117146	2.16	1834	0.09	60	74	1.36	40.71	1.14	37.20	43.14
L60-EP1-FC390-S1_2	50.0	10.0	25.0	2.01	183605	2.06	1834	0.09	60	87	1.26	50.90	1.09	47.28	51.10
L60-EP2-FC230-S1_2	50.0	10.0	25.0	1.84	117146	2.05	537	0.37	60	130	1.85	42.27	2.10	45.02	49.57
L60-EP2-FC390-S1_2	50.0	10.0	25.0	1.71	183605	1.93	537	0.37	60	146	1.73	48.86	2.01	52.57	48.41
Lam [23]															
P-2-50-1/2	50.8	12.4	50.8	2.44	176061	0.61	1679	0.07	50	54	0.76	94.24	0.50	76.11	95.48
P-3-50-1/2	50.8	12.4	50.8	3.66	176061	0.59	1679	0.07	50	61	0.73	118.80	0.49	97.34	111.70
P-1-50-1/2	50.8	12.4	50.8	1.22	176061	0.55	1679	0.07	50	39	0.83	65.61	0.50	50.75	70.32
P-1-75-1/2	50.8	12.4	50.8	1.22	176061	0.49	1679	0.07	75	37	1.22	79.71	0.71	60.83	70.91
P-2-50-1/4	50.8	6.1	50.8	2.44	176061	0.60	1679	0.07	50	48	0.85	112.29	0.55	90.52	93.86
Wu [24]															
A70	50.0	20.0	50.0	1.45	478730	0.34	699	0.43	70	79	1.89	185.85	1.73	177.70	178.88
A50	50.0	20.0	50.0	1.45	478730	0.36	699	0.43	50	81	1.37	152.31	1.27	146.61	137.23
A30	50.0	20.0	50.0	1.45	478730	0.35	699	0.43	30	80	0.82	104.36	0.75	100.12	72.97
S50	50.0	20.0	50.0	1.45	478730	0.43	1679	0.07	50	57	0.64	107.66	0.40	85.23	136.35
S30	50.0	20.0	50.0	1.45	478730	0.34	1679	0.07	30	51	0.37	78.45	0.22	60.43	58.51
S80	50.0	20.0	50.0	1.45	478730	0.35	1679	0.07	80	52	0.98	135.56	0.59	104.77	158.07
S70	50.0	20.0	50.0	1.45	478730	0.40	1679	0.07	70	55	0.88	128.04	0.54	100.52	126.44
Bocciarelli [36]															

D1	30.0	10.0	30.0	1.40	197000	0.65	1679	0.07	30	46	0.44	31.94	0.27	24.88	39.73
D2	30.0	10.0	30.0	1.40	197000	0.65	1679	0.07	30	46	0.44	31.94	0.27	24.88	42.16
D3	30.0	10.0	30.0	1.40	197000	0.65	1679	0.07	30	46	0.44	31.94	0.27	24.88	43.39
E1	30.0	10.0	30.0	1.40	197000	0.80	1679	0.07	60	51	0.91	47.65	0.58	38.04	48.75
E2	30.0	10.0	30.0	1.40	197000	0.80	1679	0.07	60	51	0.91	47.65	0.58	38.04	44.40
E3	30.0	10.0	30.0	1.40	197000	0.80	1679	0.07	60	51	0.91	47.65	0.58	38.04	45.23
L1	60.0	10.0	60.0	1.40	197000	0.80	1679	0.07	60	51	1.08	103.92	0.73	85.59	91.21
L2	60.0	10.0	60.0	1.40	197000	0.80	1679	0.07	60	51	1.08	103.92	0.73	85.59	96.70
L3	60.0	10.0	60.0	1.40	197000	0.80	1679	0.07	60	51	1.08	103.92	0.73	85.59	96.78
Al-Mosawe [27]															
S2-30	40.0	10.0	10.0	1.40	159400	0.50	699	0.43	30	57	0.73	10.88	0.57	9.62	15.52
S2-40	40.0	10.0	10.0	1.40	159400	0.50	699	0.43	40	57	0.98	13.14	0.76	11.62	20.43
S2-50	40.0	10.0	10.0	1.40	159400	0.50	699	0.43	50	57	1.22	14.96	0.95	13.23	25.70
S3-30	40.0	10.0	20.0	1.40	159400	0.50	699	0.43	30	57	0.87	24.35	0.72	22.21	41.00
S3-40	40.0	10.0	20.0	1.40	159400	0.50	699	0.43	40	57	1.16	29.40	0.96	26.81	50.70
S3-50	40.0	10.0	20.0	1.40	159400	0.50	699	0.43	50	57	1.45	33.47	1.21	30.53	60.00
NS-30	40.0	10.0	20.0	1.40	203000	0.50	699	0.43	30	63	0.84	26.76	0.71	24.67	41.90
NS-40	40.0	10.0	20.0	1.40	203000	0.50	699	0.43	40	63	1.12	32.62	0.95	30.08	51.70
NS-50	40.0	10.0	20.0	1.40	203000	0.50	699	0.43	50	63	1.40	37.34	1.19	34.43	60.70
NS-60	40.0	10.0	20.0	1.40	203000	0.50	699	0.43	60	63	1.68	41.34	1.43	38.12	69.80
UHS-30	40.0	10.0	20.0	1.20	457800	0.50	699	0.43	30	80	0.78	35.36	0.70	33.59	31.76
UHS-40	40.0	10.0	20.0	1.20	457800	0.50	699	0.43	40	80	1.04	44.26	0.94	42.04	43.30
UHS-50	40.0	10.0	20.0	1.20	457800	0.50	699	0.43	50	80	1.30	51.54	1.17	48.95	54.40
UHS-60	40.0	10.0	20.0	1.20	457800	0.50	699	0.43	60	80	1.56	57.66	1.41	54.76	64.10
UHS-70	40.0	10.0	20.0	1.20	457800	0.50	699	0.43	70	80	1.82	62.97	1.64	59.81	73.20
UHS-80	40.0	10.0	20.0	1.20	457800	0.50	699	0.43	80	80	2.08	67.71	1.88	64.32	73.20
S2-60	40.0	10.0	10.0	1.40	159400	0.50	699	0.43	60	57	1.46	16.51	1.14	14.60	27.63
S2-70	40.0	10.0	10.0	1.40	159400	0.50	699	0.43	70	57	1.71	17.89	1.33	15.82	32.62
S2-80	40.0	10.0	10.0	1.40	159400	0.50	699	0.43	80	57	1.95	19.15	1.52	16.93	30.43
S3-60	40.0	10.0	20.0	1.40	159400	0.50	699	0.43	60	57	1.74	36.94	1.45	33.69	69.10
S3-70	40.0	10.0	20.0	1.40	159400	0.50	699	0.43	70	57	2.03	40.02	1.69	36.50	76.50
NS-70	40.0	10.0	20.0	1.40	203000	0.50	699	0.43	70	63	1.96	44.87	1.66	41.37	75.00
Al-Zubaidy [28]															
CF-1-MB-1	50.0	5.0	50.0	0.17	227000	0.50	832	0.31	10	23	0.46	17.12	0.33	14.42	19.30
CF-1-MB-1	50.0	5.0	50.0	0.17	227000	0.50	832	0.31	20	23	0.93	26.94	0.66	22.69	33.40
CF-1-MB-2	50.0	5.0	50.0	0.17	227000	0.50	832	0.31	20	23	0.93	26.94	0.66	22.69	31.70
CF-3-MB-1	50.0	5.0	50.0	1.50	76652	0.50	832	0.31	10	37	0.37	23.86	0.29	21.13	30.50
CF-3-MB-2	50.0	5.0	50.0	1.50	76652	0.50	832	0.31	10	37	0.37	23.86	0.29	21.13	24.20
CF-3-MB-1	50.0	5.0	50.0	1.50	76652	0.50	832	0.31	20	37	0.75	42.64	0.59	37.76	42.10
CF-3-MB-2	50.0	5.0	50.0	1.50	76652	0.50	832	0.31	20	37	0.75	42.64	0.59	37.76	56.20
CF-3-MB-3	50.0	5.0	50.0	1.50	76652	0.50	832	0.31	20	37	0.75	42.64	0.59	37.76	49.70
CF-3-MB-1	50.0	5.0	50.0	1.50	76652	0.50	832	0.31	30	37	1.12	55.09	0.88	48.79	60.80
CF-3-MB-2	50.0	5.0	50.0	1.50	76652	0.50	832	0.31	30	37	1.12	55.09	0.88	48.79	69.70
CF-3-MB-3	50.0	5.0	50.0	1.50	76652	0.50	832	0.31	30	37	1.12	55.09	0.88	48.79	72.00
CF-1-MB-1	50.0	5.0	50.0	0.17	227000	0.50	832	0.31	30	23	1.39	33.37	0.98	28.10	29.50
CF-1-MB-2	50.0	5.0	50.0	0.17	227000	0.50	832	0.31	30	23	1.39	33.37	0.98	28.10	50.40
CF-1-MB-3	50.0	5.0	50.0	0.17	227000	0.50	832	0.31	30	23	1.39	33.37	0.98	28.10	39.30
CF-1-MB-1	50.0	5.0	50.0	0.17	227000	0.50	832	0.31	40	23	1.85	38.58	1.31	32.49	36.10

CF-1-MB-2	50.0	5.0	50.0	0.17	227000	0.50	832	0.31	40	23	1.85	38.58	1.31	32.49	40.90
CF-1-MB-3	50.0	5.0	50.0	0.17	227000	0.50	832	0.31	40	23	1.85	38.58	1.31	32.49	45.00
CF-1-MB-1	50.0	5.0	50.0	0.17	227000	0.50	832	0.31	50	23	2.31	43.14	1.64	36.33	33.80
CF-1-MB-2	50.0	5.0	50.0	0.17	227000	0.50	832	0.31	50	23	2.31	43.14	1.64	36.33	45.40
CF-1-MB-3	50.0	5.0	50.0	0.17	227000	0.50	832	0.31	50	23	2.31	43.14	1.64	36.33	43.80
CF-1-MB-1	50.0	5.0	50.0	0.17	227000	0.50	832	0.31	60	23	2.78	47.25	1.97	39.80	32.70
CF-1-MB-2	50.0	5.0	50.0	0.17	227000	0.50	832	0.31	60	23	2.78	47.25	1.97	39.80	44.10
CF-1-MB-3	50.0	5.0	50.0	0.17	227000	0.50	832	0.31	60	23	2.78	47.25	1.97	39.80	43.80
CF-1-MB-1	50.0	5.0	50.0	0.17	227000	0.50	832	0.31	70	23	3.24	51.04	2.30	42.99	33.60
CF-1-MB-2	50.0	5.0	50.0	0.17	227000	0.50	832	0.31	70	23	3.24	51.04	2.30	42.99	45.60
CF-1-MB-3	50.0	5.0	50.0	0.17	227000	0.50	832	0.31	70	23	3.24	51.04	2.30	42.99	44.50
CF-1-MB-1	50.0	5.0	50.0	0.17	227000	0.50	832	0.31	80	23	3.70	54.57	2.63	45.96	29.10
CF-1-MB-2	50.0	5.0	50.0	0.17	227000	0.50	832	0.31	80	23	3.70	54.57	2.63	45.96	45.10
CF-1-MB-3	50.0	5.0	50.0	0.17	227000	0.50	832	0.31	80	23	3.70	54.57	2.63	45.96	44.40
CF-3-MB-1	50.0	5.0	50.0	1.50	76652	0.50	832	0.31	40	37	1.50	64.49	1.17	57.12	80.60
CF-3-MB-2	50.0	5.0	50.0	1.50	76652	0.50	832	0.31	40	37	1.50	64.49	1.17	57.12	74.20
CF-3-MB-3	50.0	5.0	50.0	1.50	76652	0.50	832	0.31	40	37	1.50	64.49	1.17	57.12	81.80
CF-3-MB-1	50.0	5.0	50.0	1.50	76652	0.50	832	0.31	50	37	1.87	72.36	1.47	64.09	78.60
CF-3-MB-2	50.0	5.0	50.0	1.50	76652	0.50	832	0.31	50	37	1.87	72.36	1.47	64.09	69.20
CF-3-MB-3	50.0	5.0	50.0	1.50	76652	0.50	832	0.31	50	37	1.87	72.36	1.47	64.09	83.00
CF-3-MB-1	50.0	5.0	50.0	1.50	76652	0.50	832	0.31	60	37	2.24	79.34	1.76	70.27	74.00
CF-3-MB-2	50.0	5.0	50.0	1.50	76652	0.50	832	0.31	60	37	2.24	79.34	1.76	70.27	78.20
CF-3-MB-3	50.0	5.0	50.0	1.50	76652	0.50	832	0.31	60	37	2.24	79.34	1.76	70.27	72.50
CF-3-MB-1	50.0	5.0	50.0	1.50	76652	0.50	832	0.31	70	37	2.62	85.71	2.05	75.92	80.30
CF-3-MB-2	50.0	5.0	50.0	1.50	76652	0.50	832	0.31	70	37	2.62	85.71	2.05	75.92	70.70
CF-3-MB-3	50.0	5.0	50.0	1.50	76652	0.50	832	0.31	70	37	2.62	85.71	2.05	75.92	75.50
CF-3-MB-1	50.0	5.0	50.0	1.50	76652	0.50	832	0.31	80	37	2.99	91.64	2.35	81.16	77.00
CF-3-MB-2	50.0	5.0	50.0	1.50	76652	0.50	832	0.31	80	37	2.99	91.64	2.35	81.16	74.50
CF-3-MB-3	50.0	5.0	50.0	1.50	76652	0.50	832	0.31	80	37	2.99	91.64	2.35	81.16	77.80

653